IEEE Access
Multidisciplinary ⋮ Rapid Review ⋮ Open Access Journal

Received March 24, 2021, accepted April 18, 2021, date of publication April 30, 2021, date of current version May 14, 2021.

Digital Object Identifier 10.1109/ACCESS.2021.3076792

A Mura Detection Method Based on an Improved Generative Adversarial Network

CHEN XIE[1], KECHENG YANG[1], ANNI WANG[2], CHUNXU CHEN[2], AND WEI LI[1]

[1]School of Optical and Electronic Information, Huazhong University of Science and Technology, Wuhan 430074, China
[2]Wuhan Jingce Electronic Group Company Ltd., Wuhan 430070, China

Corresponding author: Wei Li (weili@hust.edu.cn)

This work was supported by the Major Project of Science and Technology Innovation in Hubei Province under Grant 2019AAA067.

ABSTRACT Mura is defined as visual unevenness on the display panel. It can cause unpleasant feelings, so it is necessary to perform Mura inspection during the display quality test. However, Mura is quite difficult to be detected because of its irregular shape and size as well as its low contrast. To solve this practical problem, we proposed a GAN-based model named UADD-GAN to detect Mura in this work. Consisting of a proposed UADD generator and a discriminator, the model is trained using only normal samples, after which the generator is able to simulate the distribution of normal samples. During training, the generator takes normal images as inputs and outputs their reconstructions, while the discriminator receives images and determines whether they are original or reconstructed ones, defiantly helping the generator to perform reconstructions better. The symmetric structure and the skip-adding operation make it easy for the UADD generator to reconstruct the normal samples well. In the detecting procedure, the generator performs worse in the reconstruction of samples with Mura so that we can distinguish them from the normal ones. To make full use of discriminator, we use multiple feature layers of the discriminator for supervision instead of using only the classification layer, helping the generator to reconstruct normal samples better. Meanwhile, a two-side detecting method was used to detect Mura since all the samples are not in a square shape and it greatly improved the detecting accuracy. We have conducted experiments of Mura data sets with different proportion and our research indicates that our proposed method surpasses other state of the art methods.

INDEX TERMS Mura detection, multiple supervision, UADD generator.

I. INTRODUCTION

Mura refers to the phenomenon of uneven display brightness resulting in traces on the screen. There are different kinds of Mura, which result from reasons such as poor raw materials, substrate, oil droplets dirt and so on [1]–[3]. All these Mura causes unpleasant feelings when people look at the screen. Thus, it is an important task to detect Mura as products using LCD and OLED are more and more widely used in daily life. According to the latest statistics, the global output value of display panels has reached 1146 dollars. However, the inspections of most panels at present are performed by human observers, which is very inefficient and unhealthy. Thus, we hope to improve the machine-vision based method to provide stable detection and this is a premise of Demura.

The feature of Mura is quite different from other defects. It has irregular shape and sometimes extremely low contrast, making the detection of Mura difficult. Among these Mura, band-shape Mura and line-shape Mura are particularly difficult to be detected. A mainstream Mura detection method is to enhance Mura's feature directly, as described in researches [1], [4]–[11]. Different filters are applied on the images depending on cases, strengthening the boundary of Mura or making the characteristics of Mura more obvious. This method is suitable for the detection of samples with relative even background. However, in the case of some normal samples' backgrounds are not that even, background features will also be enhanced together with the Mura features, resulting in a decrease in detection accuracy.

Another Mura detection method is based on background reconstruction [6], [11]–[21]. This kind of method firstly reconstructs the background of an image, and then obtains a residual image which contains Mura information by subtracting the background image from the original one. For example, researches [11], [14], [15], [18], [19] reconstruct the image background using discrete cosine transform(DCT).

The associate editor coordinating the review of this manuscript and approving it for publication was Tomasz Trzcinski.

[13] generates the background image with average filter. Anisotropic diffusion filter is used in [12] to extract the background of an image. And in [20], method of split Bregman is proposed to obtain the background image. Using independent component analysis, a set of basic background image is obtained from some none-defect samples. Background-reconstruction-based methods also achieve good results in some Mura detection cases. However, good background reconstruction is a prerequisite for the subsequent procedure of Mura detection. Simply using a threshold to separate the background signals may not be able to reconstruct the background satisfactorily, which could lead to errors in Mura detection.

Since it is difficult to collect Mura samples, we do not have sufficient Mura samples. So methods that require plenty of data such as YOLO or RCNN are not applicable in this case. Researches [22], [23] both provide a transfer learning based method that requires less training samples to detect Mura. However, this method is only effective in the detection of samples with Mura that has high contrast such as Gap Mura, while performs poorly in the detection of band-shape Mura and line-shape Mura.

Plenty of researches have also be done to detect some special kinds of Mura. For electrical Mura, in [24], [25], by adjusting the voltage of a screen, the brightness of the screen is also changed, which helps to distinguish the location of Mura. Research [26] came up with an idea to detect the reflected light of a screen with split beam ellipsometer, so as to find the thickness Mura and friction Mura. In [27], HDR imaging and HDR characterization are used to obtained the accurate color measurements, which can sense the subtlest color detects and is suitable for the detection of color Mura. But these methods are designed for a specific kind of Mura. They are not universal enough for the most cases of Mura detection.

It is worth noting that generative adversarial network(GAN)[28] provides a new idea for anomaly detection. GAN-based method does not need to reconstruct the image background, nor does it need to segment and extract Mura. Instead, it only needs to train an image generator and a discriminator with normal data to simulate the distribution of normal samples. For example, [29] is the first research that uses GAN for anomaly detection. Its basic idea is to use normal medical image samples to learn a flow distribution in the latent space unsupervisedly with DCGAN [30], which can be used for medical anomaly detection. [31] is an improvement of [29], introducing an encoder to reduce time consumption. [32] puts forward that the BiGAN [33] can be applied for anomaly detection, which further reduces the detection time. The model of [34], whose generator consists of an encoder and a decoder while the discriminator is a decoder, is used for the detection of abnormal X-ray images in security inspection. Although the aforementioned methods are effective in their respective application cases, they are still insufficient in the simulation of normal samples' distribution, which makes their performances poor in the Mura detection.

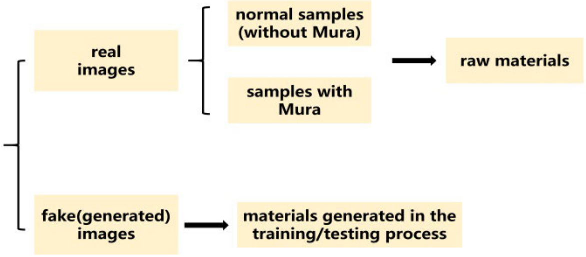
real images
normal samples (without Mura)
samples with Mura
raw materials
fake(generated) images
materials generated in the training/testing process

FIGURE 1. Relationship between some statements we use in the paper.

Motivated by the applications of GAN-based anomaly detection method in other domains [29], [31], [32], [34]–[39], we proposed a new model called UADD-GAN, to improve the accuracy of Mura detection. Our proposed method provides a new idea for Mura detection and it is particularly effective in the low-contrast Mura detection, which is difficult to be detected with traditional methods. The rest part of the paper is organized as follows. In section 2, the proposed model structure and the concrete detection method are introduced. The experiment data and some parameter setting will be elaborated in section 3. In section 4, we detect dataset of band-shaped Mura and line-shaped Mura using our proposed model, and the experimental results will be presented and discussed. Finally, conclusions are presented in section 5.

II. METHOD AND MODEL

To facilitate the introduction of the proposed model and detection method, some notations used in this paper are defined and described in Table 1. Meanwhile, Fig. 1 shows the relationships between some statements we use in the paper, giving a more intuitive picture of what they mean.

A. GAN-BASED ANOMALY DETECTION MODEL

Since Ian J. Goodfellow *et al.* proposed the generative adversarial networks in research [26], more and more people have tried to use it in anomaly detections. GAN-based framework always contains a generator and a discriminator, and it was used to generate images that look real enough at the very beginning. The generator is a network for image generation, which takes a random noise vector as input and outputs an image. On the other hand, the discriminator determines whether an image is real or not. It takes an image as input and outputs a scalar whose value is between 0 and 1, representing the image's predicted probability to be a real one. The closer it is to 0, the less possibly the input image is considered to be a real image and the closer it is to 1, the more likely the input image is considered to be a real one. When we train a GAN model, the goal of the generator is to generate as realistic images as possible to deceive the discriminator, while the discriminator tries to distinguish the generated images from the original ones. The two play against each other as shown in Fig. 2. As the game progresses, the discriminator's ability for discrimination is improved and the generator is able to generate more realistic images.

TABLE 1. Definition and description of some notations used in the paper.

Variable	description
X	The input image
G	Generator of our model
D	Discriminator of our model
P	Discriminator's prediction towards original image during training procedure
$\hat{P}$	Discriminator's prediction towards reconstructed image during training procedure
$init\_layer$	Original image's feature layers on the discriminator
$recon\_layer$	Reconstructed image's feature layers on the discriminator
$Loss\_rec$	Reconstruction loss of an image
$Loss\_pred$	Prediction loss of an image
$Loss\_\mathrm{feat}$	Feature layers' loss of an image
ω	Weight of loss
$\underset{x\sim p_x}{E}(X)$	The expectation of X under the distribution of p_x
∂	The proportion of the reconstruction loss and the feature layers' loss during testing procedure
a_score	Anomaly score of an image during testing procedure
$class$	Predicted class during testing procedure
E_X	Enhanced image
A_X	The average of an image

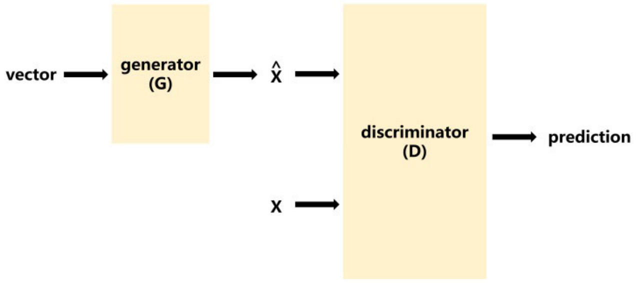

FIGURE 2. The working procedure of GAN.

We applied the GAN model to anomaly detection with some improvement on the original GAN framework. Real samples were taken as input to the generator instead of random noise. This is because the role of GAN in our method is quite different from that of an original GAN. In the original GAN, the generator receives a random vector to generate an image and there is no image comparison in the process. However, under the modified framework, the generator receives a real image and outputs its reconstructed image. We must compare the difference between the input and the reconstructed image to determine whether the input is a Mura sample or not. If we use random noise as input, image comparison will not be able to proceed. That is to say, the discriminator is used to supervise the reconstruction of the generator. When we train a model, only normal samples are used for training and the iterative training enables the generator to perfectly simulate the distribution of normal samples. During detection process, if we input a normal image, the generator can reconstruct the image well because it has come cross samples with similar feature during the training procedure. On the contrary, the input will be poorly reconstructed if it is an image with Mura. According to the different reconstruction quality, we can distinguish an abnormal image. The GAN-based anomaly detection process is shown in Fig. 3.

As a GAN-based model, our proposed model consists of two parts: a generator and a discriminator. We improved the structure of the generator and the supervision mode of the discriminator. In addition, a new detection method is designed to improve the detection accuracy when the samples are with none-square shape.

B. STRUCTURE OF OUR MODEL

1) STRUCTURE OF THE GENERATOR

We propose a U-shape generator called UADD, and its structure is shown in Fig. 4. It originates from the U-net structure and is improved to reduce the size of network and reconstruct images better. The reason we call it UADD is that it is the skip-adding operation that is used in the network rather

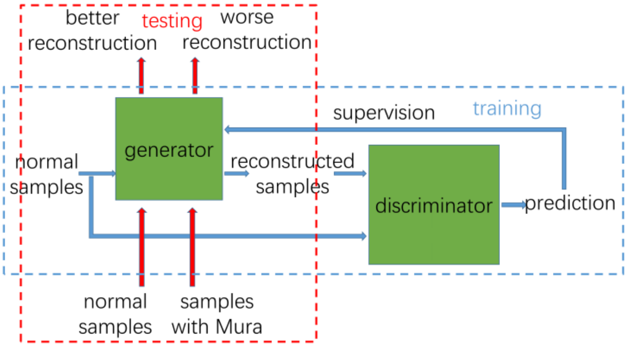

FIGURE 3. Training and testing procedure of a GAN-based anomaly detection model.

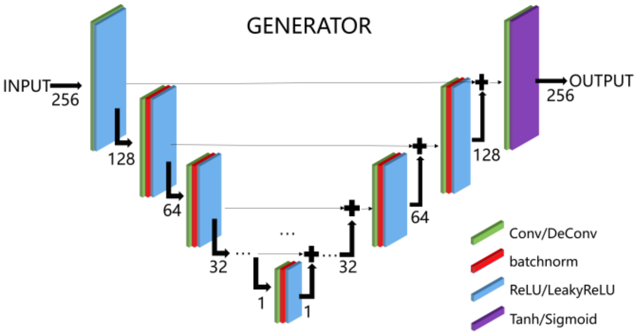

FIGURE 4. Structure of the generator. The block in green represents the convolution module, the block in red represents the normalization module, the block in blue represents the ReLU activation function and the block in purple represents the Tanh function. The number below each arrow represents the resolution of that temporal feature layer.

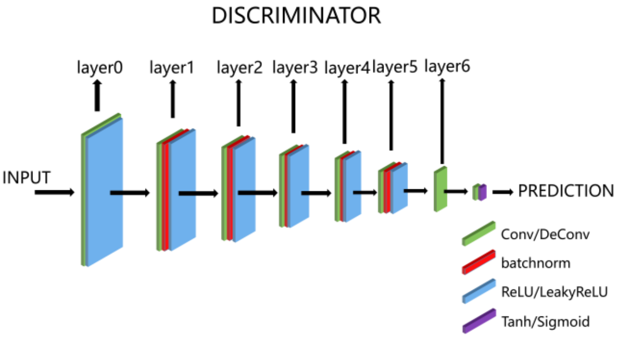

FIGURE 5. Structure of the discriminator. The block in blue represents the convolution module, the block in red represents the normalization module, the block in yellow represents the ReLU activation function and the block in purple represents the Sigmoid function. The number below each arrow represents the resolution of that temporal feature layer.

than the skip-concatenating operation. Three main techniques including down-sampling, up-sampling and skip-adding are used in the network. As shown in Fig. 4, with the generator down-sampling the input image for several times, the size of feature layers becomes smaller, which is conducive to the extraction of deep features of the image. After the last down-sampling, the generator performs up-samplings for the same times as down-sampling, forming a U-shaped structure. During up-sampling, skip-adding is adopted for feature layers with the same resolution, that is, the input of the up-sampling layer is the sum of the upper up-sampling layer's output and the output of the down-sampling layer with the same resolution. The network not only enhances the constraint on image reconstruction compared with U-net, but also reduces the parameters of model. Except for the first down-sampling layer and the last up-sampling layer, each sampling layer is composed of a convolution layer, a normalization layer and an activation layer. The input of the UADD generator must be a square-shaped image and after the last up-sampling, it can be restored to the same size as the input image. UADD generator gives a prediction for each pixel, and the skip-adding operation contributes to the reconstruction of the input image because it retains the spatial information. Combined with the discriminator, the generator learns the distribution of normal samples in an unsupervised and adversarial manner.

2) STRUCTURE OF THE DISCRIMINATOR

We adopt DCGAN's discriminator, which is classical in the GAN framework, to be our discriminator. The structure of the network is shown in Fig. 5. We explored different supervision mode of the discriminator on Mura detection. Traditionally, the discriminator receives an image, down-samples it to obtain its deep level characteristic, finally gives a classification result. This result of classification will be used to supervise the generator to help it reconstruct image better. However, supervision with only the classification result may be too weak, especially for data sets with features that have slight difference in brightness like Mura samples. Therefore, unlike the traditional supervision mode, our discriminator outputs each feature layer of the image as well instead of outputting only the classification results. Layer 0 to layer 6 in Fig. 5 represent the feature layer after the first to seventh down-sampling respectively. These feature layers will also be used for supervision along with the classification results.

The feature layers of the discriminator play a key role in the testing procedure as well. When determining whether an input image is an image with Mura, we not only take the difference between the original and reconstructed image into account, but also compare the gap of their feature layers. This comparison makes the detection more accurate.

C. TRAINING PROCESS

The training process is iterative. In a specific iteration, the training of generator and the training of discriminator are carried out alternately, playing against each other. The generator receives an image and reconstructs it as shown in (1). While the discriminator receives an image which could be real or fake, outputs its classification as well as its feature layers, as shown in (2).

$$\hat{X} = G(X) \tag{1}$$

$$\begin{cases} p, init\_layer_0, \ldots, init\_layer_6 = D(X) \\ \hat{p}, recon\_layer_0, \ldots, recon\_layer_6 = D(\hat{X}) \end{cases} \tag{2}$$

As shown earlier, we not only use the classification for supervision, but make using of different feature layers of the discriminator while training. To this end, we define the following three kinds of losses for better description of the training procedure: $Loss\_rec$, $Loss\_pred$, $Loss\_feat$.

$Loss\_rec$ refers to the difference between the original image and the reconstructed image generated by the generator. The two images have the same size. During training, $Loss\_rec$ should be reduced as much as possible to improve the generator's reconstruction ability. We use L2 distance to calculate the reconstruction loss as shown in (3),

$$Loss\_rec = \omega_{rec} mean(|X - \hat{X}|_2) \tag{3}$$

where ω_{rec} represents the weight of reconstruction loss.

$Loss\_pred$ refers to the loss caused by discriminator's wrong prediction on an image. We hope that the discriminator gives a prediction as close to 0 as possible for an original image X, and gives a prediction as close to 1 as possible for a reconstructed image $\hat{X}$, but it may give a wrong judgement resulting in the prediction loss. $Loss\_pred$ can be calculated according to (4) and we use cross-entropy loss to calculate the expectation. ω_{pred} represents the weight of prediction loss. In the training procedure, we try to reduce the prediction loss to improve discriminator's ability.

$$Loss\_pred = \omega_{pred}(\underset{x \sim p_x}{E}[\log(1-p)] + \underset{x \sim p_x}{E}[\log(\hat{p})]) \tag{4}$$

$Loss\_feat$ refers to the difference between the feature layers of an original image and its reconstructed image. In our research, with an input size of 256∗256, the discriminator has 7 feature layers. L2 distance is used to define each feature layer's loss as shown in (5),

$$Loss\_feat = \sum_{i=0}^{6} \omega_i |init\_layer_i - recon\_layer_i|_2 \tag{5}$$

where $init\_layer_i$ refers to the i^{th} feature layer of an original image, $recon\_layer_i$ refers to the i^{th} feature layer of the corresponding reconstructed image and ω_i stands for the i^{th} weight. For sake of convenience, we set ω_i as 1.

While training the discriminator, we optimize the objective function shown in (6) using gradient descent.

$$\min(Loss\_pred + Loss\_feat) \tag{6}$$

During the training process of generator, we optimize the objective function shown in (7).

$$\min(Loss\_rec + Loss\_pred + Loss\_feat) \tag{7}$$

D. DETECTING PROCESS

After being trained, the model is able to detect Mura samples. The generator takes an image as input and outputs its reconstruction while the discriminator outputs the feature layers, after which we can calculate its anomaly score a_score using (8). As shown in (8), feature loss contributes to a_score as well, which indicates the gap of deep feature between an original image and its reconstruction.

$$a\_score = Loss\_rec + \partial loss\_feat \tag{8}$$

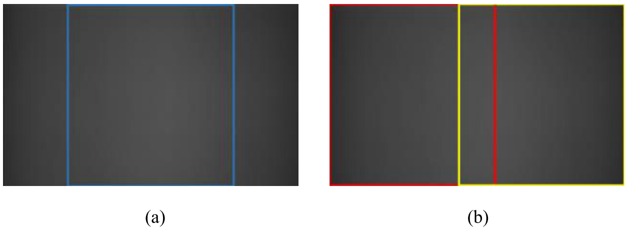
(a)

(b)

FIGURE 6. (a) Center-cropped detection method, only the area in the center that is surrounded by blue line is detected; (b) two-end detection method, area surrounded by yellow line and area surrounded by red are both detected.

For both the generator and the discriminator, the input image shape must be a square one. So the samples must be preprocessed because all of them are non-square ones. The detecting process in [32], [35], [38] uses the Center-Cropped method, that is, the middle part of the sample is extracted for detecting, as shown in Fig. 6(a). However, this kind of detecting method has a shortcoming. Some samples with Mura features that locate on the side will be judged as normal samples because the sample features are not detected, which reduces the detection accuracy. In order to solve this problem, we designed a two-end detection method that divides the image into two squares and detects both of them, as shown in Fig. 6(b). The two square images may overlap, and the model obtains the anomaly scores of them respectively, taking the bigger score as the anomaly score of the input image, as shown in (9). Plenty of experiments show that this processing method significantly improves the detection accuracy.

$$a\_score = \max\{a\_score_{left}, a\_score_{right}\} \tag{9}$$

We can set a certain threshold T and determine if an image is a sample with Mura, according to its anomaly score. As shown in (10), we determine that the input image is a sample with Mura when its anomaly score is bigger than T; otherwise, we determine it to be a normal image.

$$class = \begin{cases} normal\ sample, & a\_score \leq T \\ sample\ with\ Mura, & a\_score > T \end{cases} \tag{10}$$

E. PSEUDO-CODE

The pseudo-code of the whole procedure is as follow. In the pseudo code, G stands for generator, D stands for discriminator, "norm" stands for normal, "recon" stands for reconstruction and "loss_func" means loss function.

III. EXPERIMENT

A. DATA

The screen samples used in our experiment are provided by an institution we cooperate with and these samples come from different panel manufacturers, so they are representative. The raw data includes 286 normal samples, 308 samples with band-shape Mura and 88 samples with line-shape Mura. Fig. 7 shows a normal image, a band-shape Mura image and a line-shape Mura image respectively. The original images are in rectangle shape with an aspect ratio of 27:16. With

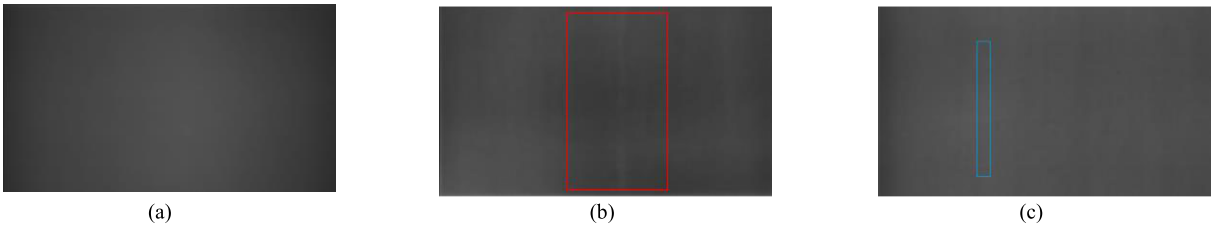

FIGURE 7. (a) normal image; (b) image with band-shape Mura, Mura locates in the area surrounded by red line; (c) image with line-shape Mura, Mura locates in the area surrounded by blue line.

TABLE 2. Pseudo code of the algorithm.

```
Training process
While iterationNumber < maxIteration:
    normRecon = G(normInitial)
    real_layers…, pred_Initial = D(normInitial)
    recon_layers, …, pred_Recon = D(normRecon)
    loss_pred = loss_func (pred_Initial, pred_Recon)
    loss_feat = loss_func (real_layers, recon _layers)
    loss_recon = loss_func (normInitial, normRecon)
    loss = loss_pred + loss_feat + loss_recon
    minimize the loss and update the model
save the best model.
Detecting process
recon = G_best(initialImage)
real_layers, _ = D_best(initialImage)
recon_layers, _ = D_best(recon)
anomaly_score = loss_func (real_layers, recon_layers)
                + loss_func (initialImage, recon)
if anomaly_score > threshold:
    initialImage is a Mura sample.
else:
    initialImage is a normal sample.
```

non-square shape, all these samples need to be preprocessed before the training and detecting procedure.

B. DATA SET MAKING AND PARAMETER SETTING

All the raw samples are resized to a proper size in the beginning. To make data sets for the detection of band-shape Mura, we selected 86 normal samples randomly as our training data. We believe that all parts of the normal samples are uniform enough so that new samples extracted from these normal samples are also free of Mura. Therefore, we randomly intercept square areas from these normal samples to expand our training data. The side length of the intercepted square is the same as the shorter side of the original samples. For testing sets, we select different number of samples from band-shape data, together with the remaining 200 normal samples to make sets of different proportions. For convenience, the proportions between Mura samples and normal samples include 10%, 20%, 25%, 33%, 50% and 75%. Because the feature of band-shape Mura is quite slight, we enhanced the contrast of all images during training and testing using (11).

$$E\_X = (1+\beta)X + (-\beta)A\_X \tag{11}$$

where β is a coefficient whose value is between 0 and 1 to adjust the image's contrast.

We use a similar method to make data sets for the detection of line-shape Mura. Interception is used to expand the training data. And we select different number of samples with line-shape Mura randomly to make testing sets with different proportions. The proportions include 10%, 20%, 30%, 40%, 50% and 75%.

The experiment is realized with Pytorch. During the training process, Adam optimizer provided by Pytorch is used to optimize the objective function. The batch size is set to 16. For the band-shape Mura data sets, the learning rates of the generator and the discriminator are both set to 0.0001, while for the line-shape Mura data sets, the learning rate is set to 0.001. We have conducted a plenty of experiments and it came out that the model was able to obtain the highest detection accuracy within 150 epochs, so we set the iteration number to 150. Weights of losses are set as follows: $\omega_{rec} = 50$, $\omega_{pred} = 1$, $\omega_i = 1$. Until stated otherwise, default settings of our experiments are set to the aforementioned values. All these experiments are carried out using a i7-9750H processor and a GeForce RTX2070 GPU.

C. CRITERIA

The receiver operating characteristic curve(ROC) is a curve drawn based on a series of different binary classification thresholds, which takes true positive rate(TPR) as its ordinate and false positive rate(FPR) as its abscissa. Area under curve(AUC) is defined as the area surrounded by the ROC curve and the coordinate axis. It represents the probability that the positive examples are ranked before the negative example. So it is applicable for the detection of imbalanced data sets and that is why AUC is cited as a detection indicator in [34]–[41]. In our experiment, we also use AUC to evaluate the detection accuracy. The closer it is to 1.0, the more accurate the detection model will be.

IV. RESULT

A. DETECTION RESULTS OF BAND-SHAPE MURA WITH FFT, TRANSFER LEARNING AND OUR GAN-BASED MEHTOD

We conducted experiments with traditional method which extracts the Mura in frequency domain. The first step was converting a sample to a frequency-domain image with FFT. We then filtered the background information with a high-pass kernel. Finally, the filtered image was converted back to the space domain with iFFT, with only the Mura information.

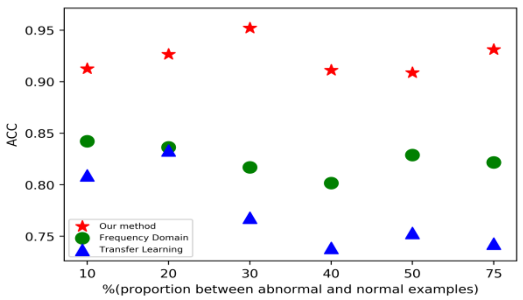

FIGURE 8. Detection accuracy of different method for different dataset.

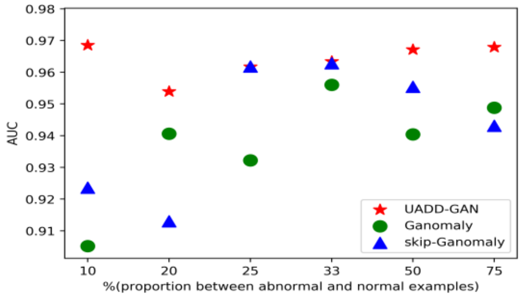

FIGURE 9. Comparison of models' detection accuracy on band-shape Mura data sets with different generators.

With a proper threshold, we can judge if there is Mura in the initial sample. Meanwhile, transfer-learning based method was also studied. We used the pretrained ResNet50 model provided by torchvision for Mura detection and some of our samples were used to fine-tune the model. The two methods mentioned above were compared with our proposed method and the results were shown in Fig. 8. It can be seen that the above two methods did not perform well in our dataset. The former achieved an average accuracy of 0.824 and the latter method achieved an average accuracy of 0.774, while our proposed method achieved an average accuracy of 0.923.

B. DETECTION RESULT OF BAND-SHAPE MURA WITH OUR PROPOSED METHOD

1) EFFECTIVENESS VERIFICATION OF THE GENERATOR

We first verified the effectiveness of our proposed UADD generator in band-shape Mura detection. We made a comparison with two other state of the art models, Ganomaly and Skip-Ganomaly. All parameters including input image size and learning rates are set the same to make it fair, except for the structures of the generators. Using DCGAN's discriminator, we tested band-shape Mura data sets with different proportions. Fig. 9 shows the highest detection accuracy of different generator on data sets with different proportions. Specifically, the average detection AUC of the model with UADD generator is around 0.964, while the average detection AUC of the model with Skip-Ganomaly's generator is around 0.943, and 0.937 with Ganomaly's generator. The average maximum AUC of UADD-GAN is 2.65% higher than that of Ganomaly, and 2.05% higher than that of Skip-Ganomaly.

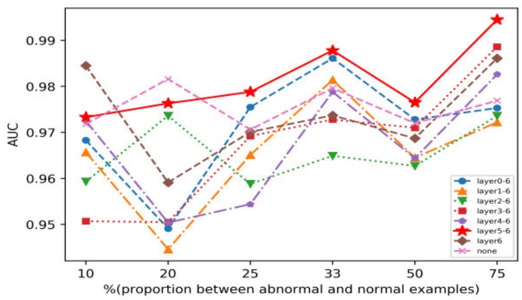

FIGURE 10. Comparison of the detection accuracy in different supervision modes.

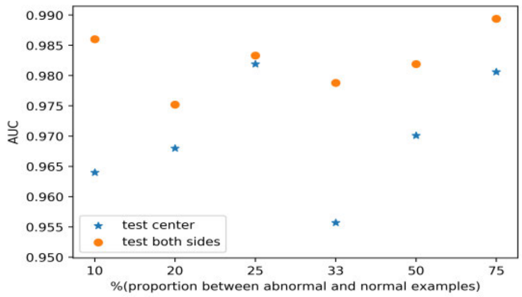

FIGURE 11. Comparison of the detection accuracy with different detecting methods.

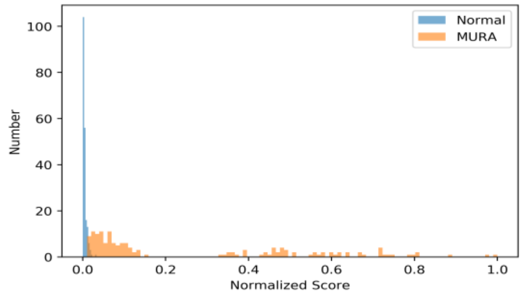

FIGURE 12. Histogram of the testing samples' normalized anomaly scores.

2) COMPARISON OF DETECTION ACCURACY IN DIFFERENT SUPERVISION MODES OF THE DISCRIMINATOR

In addition to improving the generator, we studied the influence of different supervision modes of the discriminator. Unlike the discriminator of a traditional GAN that only uses the last classification layer to supervise the generator, which may not achieve the best supervision effect, we let the feature layers take part in the supervision. For example, we have tried seven other supervision modes including classification layer + layer 6, classification layer + layer 6 + layer5, . . . , classification + layer6-layer0. For the band-shape Mura data sets mentioned before, we compared the detection accuracy. The generator we used in this experiment is the UADD generator we proposed, and the DCGAN's discriminator is used as our discriminator like before, returning the classification as well as all the feature layers. Fig. 10 shows the highest detection accuracy in different supervision modes of the discriminator. It can be seen that the overall detection accuracy for band-shape Mura data sets with different proportions reaches the

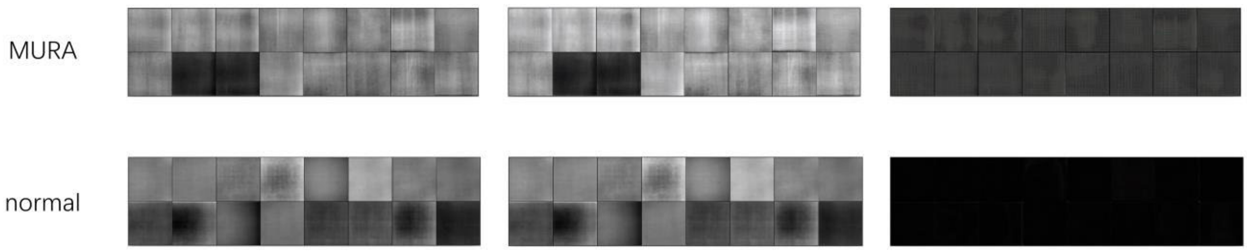

FIGURE 13. Comparison of original, reconstructed and residual images of normal samples and samples with band-shape Mura.

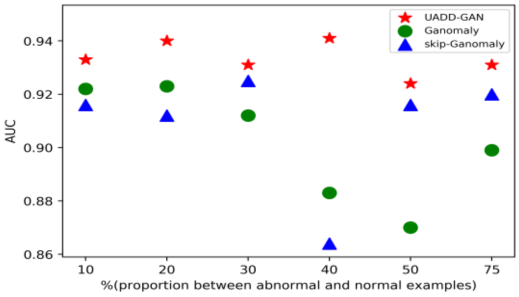

FIGURE 14. Comparison of models' detection accuracy on line-shape Mura data sets with different generators.

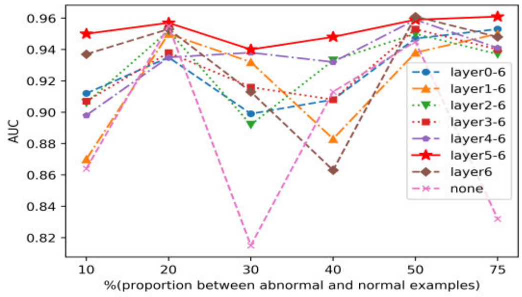

FIGURE 15. Comparison of the detection accuracy in different supervision modes.

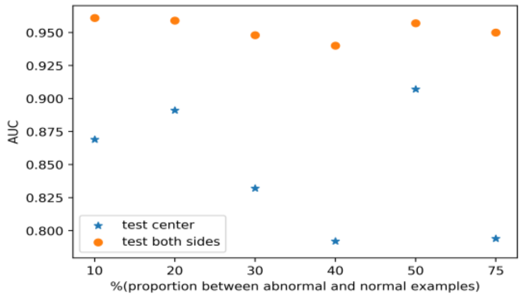

FIGURE 16. Comparison of the detection accuracy with different detecting methods.

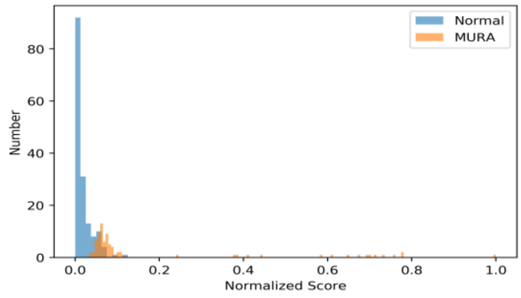

FIGURE 17. Histogram of the testing samples' normalized anomaly scores.

highest when the classification layer and the last two feature layers are used for supervision. The average highest AUC is about 0.981. If the traditional mode is used, that is, only the classification layer is used for supervision, the overall detection accuracy is around 0.965.

3) COMPARISON OF DIFFERENT DETECTING METHODS

As mentioned before, the input of the model must be images in square shape, so preprocessing is required to transform the images into square ones since all our samples are in rectangular shape. Transformation used in Ganomaly and Skip-ganomaly is based on center-cropping, which deducts the middle part of the image as input, resulting in the information loss on the two sides of the image and thus a lower detection accuracy. Therefore, we use a two-end detecting method, which crops the image from two sides and obtains their anomaly score respectively, taking the larger score as the anomaly score of the input image. We compared the two methods on band-shape Mura data sets and Fig. 11 shows the results. It turns out that the detection accuracy of the center-cropped method is around 0.964, while the accuracy of the proposed two-end detection method is around 0.982, 1.8% higher than the former one.

4) VISUALIZATION

With UADD generator and supervision mode of classification + layer 5 + layer 6, we are able to get a detection accuracy of 0.980 when the two-ends detecting is applied. Fig. 12 shows the histogram of the testing samples' normalized anomaly scores of a specific data set. It can be seen that the overall anomaly scores of normal samples are significantly smaller, ranging from 0 to 0.2. While the anomaly scores of the samples with band-shape Mura are relatively larger, ranging from 0.1 to 0.8. Given a proper threshold, we can distinguish most of the samples with band-shape Mura.

Fig. 13 shows the original images, reconstructed images and residual images of a set of normal samples and samples with band-shape Mura. It can be seen intuitively that the residual images of normal samples are darker than that of

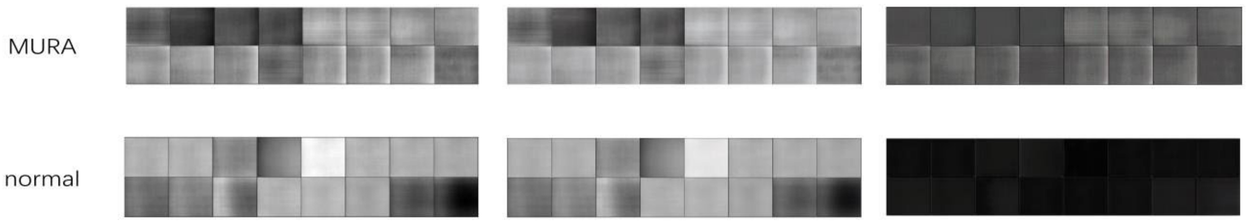

FIGURE 18. Comparison of original, reconstructed and residual images of normal samples and samples with line-shape Mura.

samples with band-shape Mura, indicating that the difference between normal samples' original images and their reconstructed images are smaller. Actually, the average gray value of the residual images of normal samples is 0.010, while the average gray value of Mura samples' residual images is 0.026, which also proves the effectiveness of our model.

C. DETECTION RESULT OF LINE-SHAPE MURA

1) EFFECTIVENESS VERIFICATION OF THE GENERATOR

Like the detection of band-shape Mura, we verified the effectiveness of our UADD generator in the line-shape Mura detection, comparing our proposed structure with the generator of Ganomaly and Skip-Ganomaly. We tested the line-shape Mura data sets with different proportion with these three models and Fig. 14 shows the highest AUC detection accuracy of different generator on data sets with different proportions. It can be seen that UADD generator has the best detection accuracy in each proportion of the data set. In fact, taking all these data sets into account, the average detection AUC of UADD generator is round 0.933, while the average AUC of Skip-Ganomaly is 0.900 and that of Ganomaly is around 0.908. In general, UADD generator achieves about 3% higher detection accuracy than the other two structures.

2) COMPARISON OF DETECTION ACCURACY IN DIFFERENT SUPERVISION MODES OF THE DISCRIMINATOR

The comparison of the detection accuracy in different supervision modes of the discriminator was also carried out on the line-shape Mura data sets with different proportions. The generator we used during the experiment was the UADD structure we proposed. Fig. 15 shows the results. It can be seen that, for the line-shape Mura data sets, the overall detection accuracy reaches the highest when the classification layer together with layer 5 and layer 6 is used for supervision. If the classification layer is the only one layer which is used for supervision, the detection accuracy declines greatly, at around 0.887, which is 7% lower than the best detection accuracy.

3) COMPARISON OF DIFFERENT DETECTING METHODS

We tested all the line-shape Mura data sets using center-cropped detection method and the proposed two-end detection method. Fig. 16 shows the accuracy of the two detecting methods on different data sets. It can be seen that the detection accuracy of the two-end detection method is greatly improved compared with the center-cropped detection method. Specifically, the AUC increases by 10.5%.

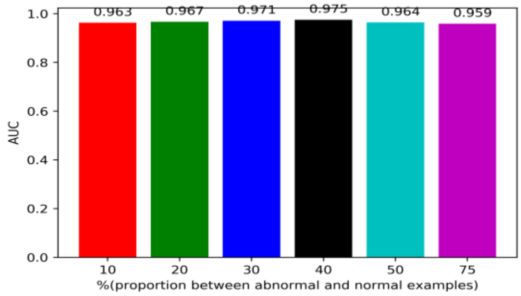

FIGURE 19. Detection AUC of the expanded dataset.

4) VISUALIZATION

We tested the line-shape Mura data set with a proportion of 50%, and Fig. 17 shows the histogram of the normalized anomaly scores. It can be seen that the anomaly scores of the normal samples are smaller. Fig. 18 shows a set of normal original images and their corresponding reconstructed images as well as residual images of a set of normal samples and samples with line-shape Mura. The average gray value of the normal samples' residual images is 0.012, and that of the line-shape Mura samples' residual images is 0.023, indicating that the generator performed better reconstructions on the normal images.

D. DETECTION RESULT OF THE EXPANDED DATASET

We extracted the areas where Mura are located with annotation tool and simply put them to the normal sample to expand the band-shape Mura dataset. In the meanwhile, we expand the normal samples by randomly cropping the initial normal samples and resizing the cropped images. In this way, we got a larger band-shape Mura dataset with 10000 normal samples and 2000 band-shape Mura samples. This method is not applicable for the expansion of line-shape Mura because it produces line-shape unevenness when the Mura area is placed in the normal sample. We have conducted experiments on the expanded dataset with our method and Fig. 19 shows the detection result. It can be seen that the AUC is still high in the detection of the expanded dataset, which indicates the effectiveness of the model more convincingly.

E. SPEED COMPARISON OF DIFFERENT MODELS

We compared our model with Ganomaly and Skip-ganomaly in terms of inference speed and the results are shown

TABLE 3. Speed comparison of different models.

models	Inference speed (ms/frame)
Ganomaly	4.66
Skip-ganomaly	5.10
UADD-GAN(classification layer+layer6+layer5) (highest accuracy)	4.81
UADD-GAN(only classification layer)	4.36
UADD-GAN(classification layer +layer6+···+layer0)	5.65

in Table 3. During the experiment, image size was set as 256∗256. It can be seen that our method is faster than Skip-ganomaly and slightly slower than Ganomaly in terms of inference speed. At the same time, with the increase of the number of supervision layers, the inference speed has decreased. For example, when only the classification layer is used for supervision, the inference speed is 4.36ms/frame, and when the classification layer together with layer6-layer0 is used, the inference speed is around 5.65ms/frame.

V. CONCLUSION

In this paper, we propose a new GAN-based anomaly detection model call UADD-GAN, to distinguish samples with Mura from the normal ones. The model consists of a generator and a discriminator. After being trained, the generator is able to perform good reconstruction for normal samples, while for samples with Mura, the reconstructed image has a large difference with the original image. Only normal samples are used in the training process, making it suitable for the cases with imbalanced data. In addition, unlike other discriminators of other GAN-based model, our discriminator utilizes features from multiple layers instead of only the final classification layers, which not only improves the supervisory ability, but helps the generator to reconstruct images better. A two-end detecting method is also proposed to avoid the omission of Mura locating in the sides of a sample, which effectively improves the detection accuracy. A large number of experiments show that our method is superior to other existing state of the art models in the given Mura data sets.

There are still some limitations in our work. For example, the detection accuracy of defect with larger shape is higher than that with smaller shape. I suggest that once a better reconstruction network is developed, it can be used in the framework so that the Mura with smaller shape can also be inspected effectively. Meanwhile traditional method can also be used together to improve the detection accuracy.

REFERENCES

[1] L. Kong, J. Shen, Z. Hu, and K. Pan, "Detection of water-stains defects in TFT-LCD based on machine vision," in *Proc. 11th Int. Congr. Image Signal Process., Biomed. Eng. Informat. (CISP-BMEI)*, Oct. 2018, p. 5.

[2] X. Xu, J. You, X. Wang, Q. Jia, Y. Wang, Y. Zhan, L. Zhang, X. Sun, J. Yang, and J. Huang, "Investigation of the color Mura mechanism and simulation models," in *SID Symp. Dig. Tech. Papers*, vol. 50, 2019, pp. 1354–1357.

[3] C.-C. Chen, S.-L. Hwang, and C.-H. Wen, "Measurement of human visual perception for Mura with some features," *J. Soc. Inf. Display*, vol. 16, no. 9, p. 969, 2008.

[4] H. Hou-Liang and Li-Wei, "Algorithm for regional Mura reduction by using gamma-curve transformation in LCD panels," in *Dig. Tech. Papers-SID Int. Symp.*, 2015, pp. 1312–1315.

[5] C.-C. Cheng and H.-M. Jao, "Application of the Haar wavelet to Mura detection for polarizer," in *Proc. IEEE Int. Conf. Ind. Technol. (ICIT)*, Feb. 2013, pp. 5–1080.

[6] Z. Ma and J. Gong, "An automatic detection method of Mura defects for liquid crystal display," in *Proc. Chin. Control Conf. (CCC)*, Jul. 2019, pp. 7722–7727.

[7] L. Miao, L. Yi-Zhi, O. Y. Jun-Lin, Y. Jian-Yong, X. Wen-Hui, and P. Li, "Automatic detection of Mura defect in TFT-LCD mobile screen based on adaptive local enhancement," *Chin. J. Liquid Crystals Displays*, vol. 33, no. 6, pp. 475–482. 2018.

[8] H. Jamleh, T.-Y. Li, S.-Z. Wang, C.-W. Chen, C.-C. Kuo, K.-S. Wang, and C. C.-P. Chen, "Automatic Mura detection based on thresholding the fused normalized first and second derivatives in four directions," *J. Soc. Inf. Display*, vol. 18, no. 12, p. 1058, 2010.

[9] L. T. Fang, H. C. Chen, I. C. Yin, S. J. Wang, C. H. Wen, and C. H. Kuo, "Automatic Mura detection system for liquid crystal display panels," *Proc. SPIE*, vol. 6070, Feb. 2006, Art. no. 60700G.

[10] Y. Sun, X. Li, and J. Xiao, "A cascaded Mura defect detection method based on mean shift and level set algorithm for active-matrix OLED display panel," *J. Soc. Inf. Display*, vol. 27, no. 1, pp. 13–20, Jan. 2019.

[11] S. Jin, C. Ji, C. Yan, and J. Xing, "TFT-LCD Mura defect detection using DCT and the dual-γ piecewise exponential transform," *Precis. Eng.*, vol. 54, pp. 371–378, Oct. 2018.

[12] Y.-C. Song and D.-H. Choi, "Anisotropic diffusion filter based blob-Mura defect detection in thin film transistor liquid crystal display panel," *Jpn. J. Appl. Phys.*, vol. 49, no. 7, Jul. 2010, Art. no. 072504.

[13] J. Kwak, K. B. Lee, J. Jang, K. S. Chang, and C. O. Kim, "Automatic inspection of salt- and-pepper defects in OLED panels using image processing and control chart techniques," *J. Intell. Manuf.*, vol. 30, pp. 1047–1055, 2019.

[14] J.-S. Park and S.-H. Lee, "Automatic Mura detection for display film using mask filtering in wavelet transform," *IEICE Trans. Inf. Syst.*, vol. 98, no. 3, pp. 737–740, 2015.

[15] Y.-B. Yang, N. Li, and Y. Zhang, "Automatic TFT-LCD Mura detection based on image reconstruction and processing," in *Proc. IEEE 3rd Int. Conf. Consum. Electron.-Berlin (ICCE-Berlin)*, Sep. 2013, pp. 240–244.

[16] K. Taniguchi, K. Ueta, and S. Tatsumi, "A Mura detection method," *Pattern Recognit.*, vol. 39, no. 6, pp. 1044–1052, Jun. 2006.

[17] S.-B. Wang, Z. J. Jhang, and C. H. Wen CH, "A Mura metric based on human vision models," in *Proc. Soc. Inf. Display-44th Int. Symp., Seminar Exhib.*, 2006, pp. 291–294.

[18] C. Ngo, Y. J. Park, J. Jung, R. U. Hassan, and J. Seok, "A new algorithm on the automatic TFT-LCD mura defects inspection based on an effective background reconstruction," *J. Soc. Inf. Display*, vol. 25, no. 12, pp. 737–752, 2017.

[19] M. Lee, S. Kim, K. Kim, W. Shin, W. Choe, and J. Kwag, "A new method for color Mura quantification," in *SID Symp. Dig. Tech. Papers*, vol. 48, 2017, pp. 1573–1575.

[20] Y.-C. Song and K.-H. Park, "Split Bregman method-based background extraction for blob-Mura defect detection in thin film transistor-liquid crystal display image," *Opt. Rev.*, vol. 18, no. 2, pp. 253–255, 2011.

[21] X. Wang, R. Dong, and B. Li, "TFT-LCD Mura defect detection based on ICA and multi-channels fusion," in *Proc. 3rd Int. Conf. Inf. Sci. Control Eng. (ICISCE)*, Jul. 2016, pp. 687–691.

[22] H. Yang, S. Mei, K. Song, B. Tao, and Z. Yin, "Transfer-learning-based online Mura defect classification," *IEEE Trans. Semicond. Manuf.*, vol. 31, no. 1, pp. 116–123, Feb. 2018.

[23] R. Singh, G. Kumar, G. Sultania, S. Agashe, P. Sinha, and C. Kang, "Deep learning based MURA defect detection," *EAI Endorsed Trans. Cloud Syst.*, vol. 5, no. 15, Jul. 2019, Art. no. 162217.

[24] Y. H. Wu, C. W. Hsu, and C. J. Chen, "A method for detecting and classifying the Mura phenomena in TFT-LCDs," in *Dig. Tech. Papers-SID Int. Symp.*, 2008, pp. 1525–1528.

[25] T.-H. Hsieh, C. Y. Hung, Y. P. Chang, and C. C. Hsu, ''Quantitative analysis of electrical Mura in LCDs,'' in *Dig. Tech. Pepers-SID Int. Symp.*, 2008, pp. 1521–1524.

[26] H. Murai, K. Ekawa, J. Takashima, H. Naito, and N. Nakatsuka, ''Mura-detection method by using a slit-beam ellipsometer,'' *J. Soc. Inf. Display*, vol. 15, no. 5, pp. 281–286, 2007.

[27] G. Nam, H. Lee, S. Oh, and M. H. Kim, ''Measuring color defects in flat panel displays using HDR imaging and appearance modeling,'' *IEEE Trans. Instrum. Meas.*, vol. 65, no. 2, pp. 297–304, Feb. 2016.

[28] I. Goodfellow, J. Pouget-Abadie, M. Mirza, B. Xu, D. Warde-Farley, S. Ozair, A. Courville, and Y. Bengio, ''Generative adversarial nets,'' in *Proc. Adv. Neural Inf. Process. Syst.*, 2014, pp. 2672–2680.

[29] T. Schlegl, P. Seeböck, S. M. Waldstein, U. Schmidt-Erfurth, and G. Langs, ''Unsupervised anomaly detection with generative adversarial networks to guide marker discovery,'' in *Information Processing in Medical Imaging*. Cham, Switzerland: Springer, 2017, pp. 146–157.

[30] A. Radford, L. Metz, and S. Chintala, ''Unsupervised representation learning with deep convolutional generative adversarial networks,'' in *Proc. 4th Int. Conf. Learn. Represent.*, 2016, pp. 1–13.

[31] H. Zenati, C. S. Foo, B. Lecouat, G. Manek, and V. R. Chandrasekhar, ''Efficient GAN-based anomaly detection,'' 2018, *arXiv:1802.06222*. [Online]. Available: http://arxiv.org/abs/1802.06222

[32] H. Zenati, M. Romain, C.-S. Foo, B. Lecouat, and V. Chandrasekhar, ''Adversarially learned anomaly detection,'' in *Proc. IEEE Int. Conf. Data Mining (ICDM)*, Nov. 2018, pp. 727–736.

[33] J. Donahue, P. Krähenbühl, and T. Darrell, ''Adversarial feature learning,'' in *Proc. 5th Int. Conf. Learn. Represent.*, 2017, pp. 1–2.

[34] S. Akcay, A. Atapour-Abarghouei, and T. P. Breckon, ''Ganomaly: Semi-supervised anomaly detection via adversarial training,'' in *Proc. Asian Conf. Comput. Vis.*, 2019, pp. 622–637.

[35] T. Schlegl, P. Seeböck, S. M. Waldstein, G. Langs, and U. Schmidt-Erfurth, ''F-AnoGAN: Fast unsupervised anomaly detection with generative adversarial networks,'' *Med. Image Anal.*, vol. 54, pp. 30–44, May 2019.

[36] J. Bian, X. Hui, S. Sun, X. Zhao, and M. Tan, ''A novel and efficient CVAE-GAN-based approach with informative manifold for semi-supervised anomaly detection,'' *IEEE Access*, vol. 7, pp. 88903–88916, 2019.

[37] M. Z. Zaheer, J.-H. Lee, M. Astrid, and S.-I. Lee, ''Old is gold: Redefining the adversarially learned one-class classifier training paradigm,'' in *Proc. IEEE/CVF Conf. Comput. Vis. Pattern Recognit. (CVPR)*, Jun. 2020, pp. 14183–14193.

[38] S. Akcay, A. Atapour-Abarghouei, and T. P. Breckon, ''Skip-GANomaly: Skip connected and adversarially trained encoder-decoder anomaly detection,'' in *Proc. Int. Joint Conf. Neural Netw. (IJCNN)*, Jul. 2019, pp. 1–8.

[39] M. Arjovsky and L. Bottou, ''Towards principled methods for training generative adversarial networks,'' in *Proc. 5th Int. Conf. Learn. Represent.*, 2017, pp. 1–17.

[40] M. Lei, Y. Zhou, L. Zhou, J. Zheng, M. Li, and L. Zou, ''Noise-robust wagon text extraction based on defect-restore generative adversarial network,'' *IEEE Access*, vol. 7, pp. 168236–168246, 2019.

[41] H. Shen, J. Chen, R. Wang, and J. Zhang, ''Counterfeit anomaly using generative adversarial network for anomaly detection,'' *IEEE Access*, vol. 8, pp. 133051–133062, 2020.

CHEN XIE received the bachelor's degree in optoelectronic information science and engineering from the Huazhong University of Science and Technology (HUST), China, in 2019, where he is currently pursuing the master's degree in optical engineering. His research interests include optical imaging, photoelectric measurement, and machine learning.

KECHENG YANG received the B.Sc. degree in optical engineering from the Huazhong University of Science and Technology, Hubei, China, in 1984, the M.Sc. degree in applied physics from Central China Normal University, Wuhan, China, in 1988, and the Ph.D. degree in physical electronics from the Huazhong University of Science and Technology, in 2000. He is currently a Professor with the School of Optical and Electronic Information, Huazhong University of Science and Technology. His research interests include optical system design, digital signal processing, and image processing.

ANNI WANG received the M.S. degree from the Ocean University of China, Qingdao, China, in 2019. She is currently an Algorithm Engineer with Wuhan Jince Electronics Group Company Ltd., Wuhan, Hubei, China. Her main research interests include deep learning and defect detection algorithm.

CHUNXU CHEN received the M.S. degree from the South China University of Technology, Guangzhou, China, in 2016. He is currently an Algorithm Engineer with Wuhan Jince Electronics Group Company Ltd., Wuhan, Hubei, China. His main research interests include deep learning and defect detection algorithm.

WEI LI received the Ph.D. degree in physical electronics jointly from the Huazhong University of Science and Technology (HUST), China, and the University of California at San Diego, San Diego, CA, USA, in 2009. She is currently an Associate Professor with the School of Optical and Electronic Information, HUST. Her research interests include optoelectronic sensing and imaging, optical scattering theory, and fiber sensing technology.